INFLUENCE OF FIBER ORIENTATION ON THE BRIDGING PERFORMANCE OF PVA FRCC

Toshiyuki Kanakubo, Masaru Miyaguchi and Kohei Asano

Biography: ACI member **Toshiyuki Kanakubo** is an Associate Professor at the Department of Engineering Mechanics and Energy, University of Tsukuba, Japan. He received his Ph.D. from University of Tsukuba. His research interests include high-performance fiber-reinforced cementitious composites (HPFRCC), the structural behavior of FRP reinforced concrete structures, and bond properties of reinforcement and concrete. He is the secretary of the Technical Committee ISO/TC71/SC6, Non-Traditional Reinforcing Materials for Concrete Structures.

Masaru Miyaguchi is a student in the master’s program at the Department of Engineering Mechanics and Energy, University of Tsukuba, Japan. He received his B.E. from University of Tsukuba, Japan. His research topic is the evaluation of fiber orientation in high-performance fiber-reinforced cementitious composites (HPFRCC), and their influence on the mechanical behavior of HPFRCC.

Kohei Asano is a Research Associate at the Department of Architecture, Miyakonojo College, National Institute of Technology, Japan. He received his Ph.D. from University of Tsukuba, Japan. His research interests include the mechanical behavior of high-performance fiber-reinforced cementitious composites (HPFRCC), and structural performance of RC members using HPFRCC.

ABSTRACT

Crack bridging performance of fibers strongly affects the tensile characteristics of fiber-reinforced cementitios composites (FRCC) after first cracking. The fiber orientation distribution is likely to be affected by factors that include fresh-state properties, casting method, formwork geometry, and others. The objective of this study is to investigate the influence of the fiber orientation on the bridging performance in polyvinyl alcohol (PVA) FRCC through a visualization simulation using a water glass solution and a calculation of the bridging law. The main parameter of the investigations, in the present study, is the casting direction. To evaluate the fiber orientation distribution quantitatively, an approximation methodology using an elliptic function is newly introduced. The bridging stress versus crack width relationship is calculated considering the elliptic distribution, the snubbing effect, and the fiber strength degradation. The calculated stress – crack width curves can express well the uniaxial tension test results after first cracking.

Keywords: FRCC; casting direction; fiber orientation; image analysis; bridging law; uniaxial tension test; elliptic function; orientation intensity

INTRODUCTION

The crack bridging performance of fibers, that is generally expressed by a bridging stress – crack opening relationship (called the bridging law), strongly affects the tensile characteristics of fiber-reinforced cementitious composites (FRCC) after first cracking. The bridging performance is characterized and/or controlled by the properties of the matrix, the fiber, and the fiber-matrix interface [1,2]. Since the 1980s, studies on high-performance fiber-reinforced cement composites (HPFRCC) and engineered cementitious composites (ECC) have been conducted to understand the crack bridging performance, primarily because these composites require the balanced properties of the matrix, the fiber and their interface, to exhibit the pseudo strain-hardening behavior [3,4]. One of the examples of a polymeric fiber bridging law is that presented by Kanda and Li [5] who described it for polyvinyl alcohol (PVA) fibers assuming the following characteristics: (1) the chemical bond in the fiber-matrix interface, (2) the rupture of the fiber, and (3) the tensile strength reduction owing to inclined-angle bridging. These considerations had primarily been introduced to account for the characteristics of randomly oriented, discontinuous fibers [6].

Many researchers have studied the effects of fiber orientation on the mechanical characteristics of FRCC, including fiber-reinforced concrete (FRC). The categories of these materials including HPFRCC and ECC are summarized in some literatures [e.g.7]. In addition, self-consolidating concrete (SCC) and ultra-high performance fiber-reinforced concrete (UHP-FRC) have been developed for the last several decades. These materials have specific properties that require researchers and engineers to be attentive to fiber orientation. The scheme of the current approach to evaluate the fiber orientation has considered the casting method, fresh-state properties, flow, vibration, and formwork geometry [8]. The cementitious matrix used in HPFRCC and ECC has a high viscosity aiding the random distribution of the fine fibers, and commonly has self-compacting properties. These characteristics indicate that the bridging law in HPFRCC and ECC is likely to be affected by the fiber orientation. In fact, the tensile characteristics of polymeric fiber-reinforced cementitious composites differ because of the casting direction and the dimension of the specimen [9]. The wall effect, in which the fiber orientation is influenced by the surface of the mold, has also been studied by many researchers. Li and Wang [10] categorized the fiber orientation as two-dimensional (2-D) random and three-dimensional (3-D) random by the specimen dimensions in two perpendicular sectional planes. The ultimate tensile strain of PVA-ECC tends to decrease if the specimen dimension changes from 2-D to 3-D.

Statistical approaches on the fiber orientation distribution began in the 1960s. Naaman [11] proposed a sinusoidal function as the probability density function (PDF) of the angle between the fiber and the normal vector of the cut plane. Stroeven [12] indicated the combination of three typical distributions, namely, 3-D random, 2-D random, and perfectly aligned one-dimensional for simulation of arbitrary orientation distributions. One of the examples of the approaches adopted to study the wall effect is presented by Dupont and Vandewalle [13]. They proposed a theoretical quantification by predicting the total number of fibers crossing a rectangular section. Considering the influence of the matrix flow, Xia and Mackie [14] proposed the probabilistic spatial orientation using the beta distribution as the axisymmetric fiber orientation. There have been lots of studies to investigate the fiber orientation and distribution by experimental approaches observing fibers directly via image-based analysis. In case of steel fibers, X-ray technique is one of the effective methods. Recently, micro-computed tomography (micro-CT) has been used to characterize the fiber distribution [15]. In case of polymeric fibers such as PVA, image analysis taking advantage of absorbing the ultraviolet radiation was conducted [16].

It is considered that the bridging performance, i.e. the tensile properties of FRCC, can be characterized using the fiber orientation distribution. The main objective of this study is to investigate the influence of fiber orientation distribution on the bridging law of polymeric fibers. The main experimental parameter selected in this study is the casting direction, which is considered to have an influence to the fiber orientation distribution.

To achieve the goal, a visualization simulation is conducted using sodium silicate solution (known as water glass) to observe the flow patterns of the fibers in the tension test specimen. The results of the visualization simulation are discussed mainly for the distribution of the angles of the fibers. In this study, based on the visualization results, a new PDF is proposed to describe variation in the fiber angle. The PDF is expressed by two parameters: the principal orientation angle and the orientation intensity. These parameters indicate the angle and the tendency of the fibers to orient along the direction of the principal orientation. Finally, the bridging law, which is obtained by a numerical calculation, is compared with the tension test results.

The fine fibers with a diameter ranging between 0.01 mm – 0.04 mm (4×10^{-4} in. – 16×10^{-4} in.) are commonly used for HPFRCC/ECC to actualize the pseudo strain-hardening behavior and multiple cracking. On the other hand, multiple cracking makes the observation of the bridging law difficult. In this study, PVA fiber with a diameter of 0.10 mm (3.9×10^{-3} in.) is utilized to observe the bridging law (tensile stress – crack width curve) directly by the tension test subjected to single crack formation.

RESEARCH SIGNIFICANCE

Evaluation of the bridging law, accounting for the fiber orientation distribution, is necessary for predicting the precise tensile characteristics of FRCC. The fiber orientation, which is affected by casting method, fresh-state properties, flow, and formwork geometry, should be considered in the manufacturing of the composites for practical uses. The bridging characteristics of polymeric fibers are affected by their angle with the cracking plane.

Understanding the fiber behavior expressed by the bridging law can facilitate understanding the tensile characteristics of FRCC. A simple mathematical expression for the PDF of the fiber orientation distribution would also simplify simulations of the bridging law.

VISUALIZATION SIMULATION OF FIBER ORIENTATION

Materials for simulation test

PVA fibers of 0.10 mm (3.9×10^{-3} in.) diameter were utilized in this study. The mechanical properties of PVA fibers are listed in Table 1. In order to visualize the flow of the fiber in a matrix, a sodium silicate solution (hereafter referred to as water glass) was adopted as the matrix. Water glass has high viscosity, and it is colorless and transparent. In regards to the practical use of ECC, the rheology of mortar matrix before mixing the fiber was inspected using the flow time [17], based on "Test method for flowability of grout for prestressing tendons (JSCE-F531-2013)" [18]. The flow time is measured using the funnel shown in Fig. 1. The flow time of water glass was controlled by adding pure water, in an effort to attain the same flow time of mortar matrix as that of the target HPFRCC. The mix proportion of the target HPFRCC is listed in Table 2. This proportion is selected for the tension test specimens, as explained in a later section. The measured flow time of the mortar matrix was 36 sec. in average for each of the eight mixture batches with the same mix proportion. The water glass to the pure water weight ratio was chosen to be 12:1 at a temperature of 25 °C. The density of the water glass solution was 1.62 g/cm^3 (101 lb/ft^3), which is smaller than 1.89 g/cm^3 (118 lb/ft^3) of mortar matrix used for the tension test specimens.

The color of PVA fibers, which is almost white, makes it difficult to distinguish them from the water glass solution. Therefore, black-colored "target fibers" made from Nylon were added to the matrix to simplify the image analysis. The mechanical properties of the target fibers are listed in Table 1. The volume fraction of the target fibers was set to 0.05%

based on empirical trial and error results. The mixture states are shown in Fig. 2. The image analysis on target fibers (explained in a subsequent subsection) was conducted based on the assumption that these fibers flow in similar orientations as those associated with the PVA fibers.

Simulation method

Water glass solution containing PVA and the target fibers was poured into the mold, using the same way as that used for HPFRCC casting. The mold was constructed with transparent acrylic plates. For simulations of the flow in the tension test specimens, the cross-section of the mold was chosen to be 40 mm × 40 mm (1.57 in. × 1.57 in.) to be over three times the fiber length of 12 mm (0.47 in.), considering 3-D orientation of fibers [10]. The testing parameters included the casting direction and the volume fraction (V_f) of the PVA fibers. The dimensions of the mold are shown in Fig. 3. Two molds were prepared, one for the casting along the horizontal direction and a second for the casting along the vertical direction. Water glass solution was poured into the mold using a bucket at the points indicated by the arrows in Fig. 3. The pouring time was approximately 20 sec. and was similar in value to the case of casting of the tension test specimens. After pouring, photos of the x-y and z-x planes were taken using two digital cameras at in-plane resolution of 6000 × 4000 pixels. The setup of the cameras for the horizontal casting simulation is shown in Fig. 4. Simulated volume fractions of PVA fibers are 0.1%, 0.5%, 1.0%, 1.5%, and 2.0%. For each volume fraction, three image specimens were cast followed by photo capturing were carried out. An example of the photograph (V_f = 0.1%, horizontal casting, z-x plane) is shown in Fig. 5.

Image analysis and calculation of fiber angle

Image analysis was conducted to obtain the fiber angles in the water glass solution. The image analysis and calculation of the fiber angles were carried out for the target fibers that occupied the central 40 mm (1.57 in.) region as shown in Fig. 5. The procedure of the image analysis is described as follows:

(1) The photograph is cropped to include only the target region. (Fig. 6 (a))

(2) The image is binarized and the noise is filtered. (Fig. 6 (b))

(3) RGB values (red-green-blue values in bit for each color) of the pixel data are read with position coordinates (X_i, Y_i).

(4) The sequences of black-colored pixels are grouped and labelled. (Fig. 6 (c))

After this process, a straight line approximation is calculated using the position coordinates of the pixels of the same group, using least-squares regression analysis by minimizing the distance between the point and the line. The fiber angle is defined as the angle between the fitted line and the longitudinal axis (x-axis). The fiber angle ranges between $-90°$ to $+90°$.

Examples of fiber angle histograms (V_f = 0.1%, horizontal casting) are shown in Fig. 7. The diagram on the right side of this figure corresponds to the calculated histogram result based on the photograph of Fig. 5, and the analysis methodology shown in Fig. 6. As indicated in Fig. 6 (b), fiber angles mostly range between 0 ° to 45 °. The frequencies of the fiber angles that are extracted based on the three-time pouring and photography are added together, and one diagram is drawn for each parameter of the simulation test. All the fiber angle histograms are shown in Fig. 8. As expected, there is a tendency that the fibers flow along the longitudinal direction in the case of horizontal casting, and along the perpendicular direction in the case of vertical casting. The presented solid lines and the respective values of the diagrams are explained in the next section.

PDF FOR FIBER ORIENTATION DISTRIBUTION

Approximation based on the elliptic function

For the purpose of quantitative evaluation of the fiber orientation distribution, an approximation methodology using the elliptic function is introduced. This methodology was studied in the field of “Japanese traditional paper (Washi)” [19]. The relative frequency for each class of fiber angle is transformed into a vector with the argument set to be equal to the fiber angle as shown in Fig. 9. The trajectory traced by the terminal points of these vectors is approximated by an ellipse fitted using the least squares method. The ellipse is expressed as a function of two radii, *a* and *b*, and the angle with respect to the *x**-axis, θ_r, as shown in the figure. The value of θ_r ranges between $-45\,°$ to $+45\,°$, and the argument of radius *a* corresponds to θ_r. As shown in Fig. 9, a random fiber orientation results in a circle whereas the orientation tendency of the fibers along the longitudinal direction results in an ellipse. As the longitudinal directionality becomes greater, the shape of the ellipse becomes narrower. The ratio of the two radii, $k = a / b$, can express the shape of the ellipse. This ratio of two radii is defined as “orientation intensity”, and the angle, θ_r, is defined as “principal orientation angle”. The orientation intensity value reflects the orientation tendency of the fibers that lie along the principal orientation angle. When the fibers orient perfectly randomly, k is equal to 1. As shown in Fig. 10, when the fibers show an increased directional orientation toward the principal orientation angle, the value of k is larger than 1. In contrast, when the fibers orient perpendicularly with respect to the principal orientation angle, the value of k is smaller than 1.

The PDF that expresses the relative frequency corresponding to the fiber angle, θ, is described by Eq. (1): hereafter, the PDF is referred to as “elliptic distribution”. The parameters for this function are the orientation intensity, *k*, and the principal orientation angle, θ_r. When θ_r is equal to zero, the elliptic function is simply given by Eq. (5). The definite integral calculus of Eq. (1) and Eq. (5) in $-\pi / 2 \le \theta \le \pi / 2$ gives 1 (the sum of probability).

$$p(\theta) = \frac{\sqrt{k}}{\pi} \cdot \frac{C}{\cos^2\theta + A\sin\theta\cos\theta + B\sin^2\theta} \tag{1}$$

$$A = \frac{(1-k)\sin 2\theta_r}{1+(k-1)\sin^2\theta_r} \tag{2}$$

$$B = \frac{k-(k-1)\sin^2\theta_r}{1+(k-1)\sin^2\theta_r} \tag{3}$$

$$C = \frac{1}{1+(k-1)\sin^2\theta_r} \tag{4}$$

$$p(\theta) = \frac{\sqrt{k}}{\pi} \cdot \frac{1}{\cos^2\theta + k\cdot\sin^2\theta} \tag{5}$$

Approximation of visualization simulation results

The results of the approximation of the fiber angle distribution obtained in the visualization simulation are shown in Fig. 8 by solid lines. The values of the orientation intensity, k, and the principal orientation angle, θ_r, are also listed in the figures. When the directionality of the fiber orientation increases along the longitudinal direction, the value of the orientation intensity is over five (cases of z-x plane for V_f = 1.0, 1.5 and 2.0%). In vertical casting, the fiber angles tend to align along the perpendicular direction, and there are the cases that the value of the orientation intensity becomes smaller than 0.5 (cases of x-y and z-x planes for V_f = 1.5 and 2.0%). These evaluations are done for two planes individually. The estimated probabilities for each plane are multiplied to express the probability in 3-D orientation in a later section.

UNIAXIAL TENSION TEST

Test outline

For verification of the influence of fiber orientation on tensile behavior, the uniaxial tension test was conducted. As explained in the Introduction, PVA fibers with a diameter of 0.10 mm (3.9×10^{-3} in.) are utilized to observe the bridging law directly, subjected to single crack formation. The mechanical properties of the PVA fiber are listed in Table 1. The fibers used for the tension test are same as those used in the visualization simulation. The mix proportion of mortar matrix has already been presented in Table 2. The fiber volume fraction is 2.0 %.

The testing parameter is the casting direction along both the horizontal and vertical directions. Two types of molds for each casting direction were prepared, as shown in Fig. 11. The matrix with fibers was poured into the mold using a bucket employing the same approach as the one used for the visualization simulation. The pouring time was controlled to be approximately 20 sec. in the test region.

The dimensions of the specimen and the specimen setup are shown in Fig. 12. The cross-section of the test region is 50 mm × 50 mm (1.97 in. × 1.97 in.) square to be over three times the fiber length of 12 mm (0.47 in.), considering 3-D orientation of fibers [10]. The total length of the specimen is 510 mm (20.1 in.). A 2,000 kN (450 kips) universal loading machine was used. Pin-fix ends were used at the boundaries to minimize possible effects of development of external moment because of setup irregularity, and secondary moment influencing local fracture [9]. The carbon fiber sheets were attached at both ends to avoid peel-off of the steel plate. Measurement items were tensile load and deformation in the test region using two pi-type displacement transducers. Two series of test in different period (Batch #1, compressive strength 39.2 N/mm^2 (5.69 ksi), and Batch #2, compressive strength 41.0 N/mm^2 (5.95 ksi)) were carried out.

Test results

All specimens fractured by a single crack. Some of the specimens had a fine crack before loading because of an unskillful treatment during the formwork removal. The test results of these specimens are excluded from the following discussions. The curves of the tensile stress – crack width are shown in Fig. 13. It is clearly recognized that the casting direction remarkably affects the tensile performance. The test results are summarized in Table 3. The average tensile stress at the maximum load after the sudden drop of the load (second peak) is 3.51 N/mm^2 (0.509 ksi) and 1.67 N/mm^2 (0.242 ksi) for the horizontal casting and the vertical casting specimens, respectively. The tensile stress of the second peak of horizontal casting specimens is more than two times that of the vertical casting specimens. The crack width at the second peak of the horizontal casting specimens is on average 1.73 times higher than the corresponding value of the vertical casting specimens.

Characteristic example photographs of the fractured surface after loading are shown in Fig. 14. It is clearly seen that the protruded fibers from the surface of the horizontal casting specimen are many more and longer than those of the vertical casting specimen.

BRIDGING LAW CONSIDERING FIBER ORIENTATION

Trilinear model for pullout load versus crack width relationship

The calculations of the bridging law of the PVA fiber considering the fiber orientation distribution are conducted. The elliptic distribution expressed by the orientation intensity and the principal orientation angle is adopted for the PDF estimation of the fiber orientation distribution. The orientation intensity and the principal orientation angle used for calculations are based on these results of the visualization simulations.

The pullout properties of the single fiber are required to calculate the bridging law. Several researchers have studied the bond behavior of PVA single fiber to cementitious matrix [20-23] Table 4 lists the results from previously published studies in which the pullout tests of the single fiber were performed. It has been known that the bond behavior of the PVA fiber consists of two stages, i.e., the chemical bond stage and the friction stage [20]. The pullout load versus displacement relationships of the PVA fiber commonly exhibit the first peak in the debonding process of the chemical bond, and slip hardening or softening [21]. Table 4 lists the information of the matrix used, the fiber diameter, first peak load, and the maximum load in the friction process (second peak). Based on these results, a trilinear model is assumed to express the relationship between the pullout load and the crack width for a single fiber, as shown in Fig. 15. The pullout load for the first branch, P_a, and it for the maximum, P_{max}, corresponds to the first peak load and the second peak load, respectively. As seen in Table 4, there is no test result listed on PVA fibers with a diameter of 0.10 mm (3.9×10^{-3} in.), as used in this study. Furthermore, the water to cement ratio used in this study is 0.56, which also differs from corresponding ratio values in prior studies. Considering the differences of fiber diameters and mix proportions of the matrix, the values of P_a and P_{max} are assumed to be 1.5 N (0.34 lbf) and 3.0 N (0.67 lbf), respectively. These values correspond to the values of 0.24 N (0.054 lbf) and 0.48 N (0.108 lbf) for the same tensile stress of a PVA fiber with a diameter of 0.04 mm (1.6×10^{-3} in.). The values of 0.24 N (0.054 lbf) and 0.48 N (0.108 lbf) are in the ranges of the test results reported by Kiyota et al. [22].

The crack widths, δ_a and δ_{max}, are those corresponding to the loads of P_a and P_{max}, respectively. These crack widths correspond to the slip-out displacements at the first and second peak loads in the pullout test. The slip-out displacements for the two peaks are simply assumed to be 0.1 mm (3.9×10^{-3} in.) and 0.3 mm (12×10^{-3} in.) from the test results of Yang et al. [23]. The crack width becomes twice the slip-out displacement before the maximum load, because the fiber slips out from the both embedded sides. When the pullout load starts to decrease at the short embedded side of the fiber, the slip-out displacement at the long embedded side decreases [24]. To express this phenomenon using a simple trilinear model, the crack width at the maximum load is assumed to be 1.5 times the slip-out displacement at the second peak in the pullout test. As a result, the values of δ_a and δ_{max} are assumed to be 0.2 mm (7.8×10^{-3} in.) and 0.45 mm (18×10^{-3} in.), respectively. The softening branch is decided as the pullout load becomes zero, when the crack width equals the embedded length of the short side of the fiber, l_b. These assumed values are summarized in Table 5 and illustrated also in Fig. 15.

Bridging law simulation method

The bridging stress can be obtained as the total pullout load of fibers divided by the cross-sectional area of the matrix. Moreover, the elliptic distribution is adopted to express the fiber orientation distribution. The snubbing effect [24] and the fiber strength degradation [20] are also considered in this study. The snubbing effect exhibits the increment of the pullout load of the fiber due to the edge reaction, when the fiber has the angle with the normal direction of cracking plane. The fiber strength degradation has been adopted for the polymeric fibers, which strength decreases when the fiber is pulled out slantingly from its embedded direction.

The definitions of the coordinate system and the fiber angle in consideration of the snubbing effect and the fiber strength degradation are shown in Fig. 16. The fiber angles, θ and ϕ, are the angles between x-axis and the projected lines of the fiber (angle of ψ to x-axis) to x-y and z-x planes, respectively. When the angle ψ increases, the pullout load also increases owing to the snubbing effect. However, as this angle increases, fiber strength decreases, and the fiber ruptures easily (Fig. 15). The elliptic distribution is considered for each of the x-y and z-x planes. Therefore, the formula expressing the bridging stress can be given by Eq. (6). Eq. (6) is derived by the summation of the pullout load of the fibers which exist in bridging the crack surface with the probability given in the elliptic distribution. The probabilities for x-y and z-x planes are multiplied to express the probability in 3-D orientation. The pullout load of a single fiber, P, is given by Eq. (7), expressing the snubbing effect and the fiber strength degradation.

$$\sigma_{bridge}(\delta) = \frac{P_{bridge}(\delta)}{A_m} = \frac{V_f}{A_f} \cdot \sum_h \sum_j \sum_i P_{ij}(\delta,\psi) \cdot p_{xy}(\theta_i) \cdot p_{zx}(\phi_j) \cdot p_x(y_h, z_h) \cdot \Delta\theta \cdot \Delta\phi \cdot (\Delta y \cdot \Delta z) \tag{6}$$

$$P = P_{pull} \cdot e^{f \cdot \psi} < P_{rup} \cdot e^{-f' \cdot \psi} \text{ (once exceeded, } P = 0\text{)} \tag{7}$$

where

σ_{bridge} = bridging stress

δ = crack width

P_{bridge} = bridging force (= total of pullout load)

A_m = cross-sectional area of the matrix

V_f = fiber volume fraction

A_f = cross-sectional area of a fiber

P = pullout load of a single fiber

P_{pull} = pullout load of a single fiber at a zero fiber angle

P_{rup} = pullout load of a single fiber at rupture at a zero fiber angle

f = snubbing coefficient

f' = fiber strength reduction factor

p_{xy}, p_{zx} = probability based on elliptic distribution

p_x = probability of fiber distribution along x-axis

ψ = fiber angle to x-axis

θ = angle between x-axis and projected line of the fiber to x-y plane

ϕ = angle between x-axis and projected line of the fiber to z-x plane

The PDF, p_x (y, z), gives the probability for the existence of the fiber in the x-axis direction. In this study, p_x (y, z) is assumed to be constant. This means that the fibers are randomly distributed along the longitudinal direction of the specimen.

The input values for the parameters are listed in Table 5. The orientation intensities for the horizontal casting are selected to be 1.5 and 6 for the x-y and the z-x planes, respectively. On the other hand, the corresponding values for the vertical casting are set to 0.5. These values are chosen based on the results of the visualization simulation for V_f = 1.5% and 2.0% (Fig. 8). The principal orientation angles are set to zero for calculation simplification. This value almost agrees with the average value of all the results of the visualization simulation. The calculations were done by using a spreadsheet software.

Comparison with tension test result

The calculated curves showing the variation of the bridging stress (tensile stress) with the crack width are shown in Fig. 17 together with the tension test results, for both the horizontal and vertical casting specimens. Because the calculated curves exhibit the bridging stress by fibers after cracking, the elastic region before cracking in the tension test (indicated by dotted line) cannot be compared with the calculated curve. The calculated curves express well the test results after the first peak in the tension test. Based on these calculations, the only parameter that differs between the horizontal and vertical casting is the orientation intensity. The difference of the fiber orientation intensity identifies a clear influence on the bridging law.

Fiber effectiveness is also defined to express the effectiveness of the fiber in bridging the crack surface. It is calculated as the ratio of the number of fibers crossing the crack surface (neither slipping out nor rupturing) to the theoretical number of total fibers in a unit volume. The fiber effectiveness is equal to the orientation factor at a crack width of zero. Fig. 17 also shows the calculation results of fiber effectiveness and crack width relationship both for the horizontal and the vertical casting specimens. The fiber effectiveness values at a crack width of zero are 0.544 and 0.315 for horizontal and vertical casting, respectively. The difference of the fiber orientation distribution causes this disparity. The fiber effectiveness decreases as the crack width increases because of slipping out or because of fiber rupture. The "step" can be seen on the curve, when the fibers rupture more frequently. The balance between the increase of the pullout load and the loss of the bridging because of fiber rupture leads to the maximum bridging stress. After the end of the "step", the fiber effectiveness of horizontal and vertical casting becomes 0.346 and 0.116, respectively. These values are considered almost equal to the orientation factor after fracture, i.e., the ratio of the fibers that slipped out from the crack surface. The tension test results shown in Fig. 14 support this consideration.

CONCLUSIONS

To investigate the influence of the fiber orientation distribution on the bridging performance in PVA-FRCC, visualization simulation using water glass solution and calculation of the bridging law considering the fiber orientation distribution were conducted. The main parameter of the investigations is the casting direction of FRCC. The followings are concluded from this study.

1. From the visualization simulation, the fibers have a tendency to flow along the longitudinal direction in the case of horizontal casting and along the perpendicular direction in the case of vertical casting.
2. To evaluate the fiber orientation distribution quantitatively, a new approximation methodology using an elliptic function was introduced. The PDF named elliptic distribution is characterized by the principal orientation angle and the orientation intensity.

3. From the visualization simulation, while the value of the orientation intensity shows over five in the case of horizontal casting, there are the cases that the orientation intensity becomes smaller than 0.5 in the case of vertical casting.
4. The bridging stress versus crack width relationship was calculated considering the elliptic distribution, the snubbing effect and the fiber strength degradation. The calculated bridging curves were compared with the results of the tension test in which the specimens were fabricated by horizontal and vertical casting. The calculated curves expressed well the test results after first cracking.
5. The differences of the fiber orientation distribution clearly indicated an influence on the bridging law. Based on the calculation results for the bridging law, it was considered that the balance between the increasing pullout load and the loss of the bridging force because of the fiber rupture leads to the maximum bridging stress.

FUTURE RESEARCH

In this study, only one type of mold and matrix was utilized for the visualization simulation. It is considered that the other factors such as casting method, fresh-state properties, flow, vibration, formwork geometry have also influences to the fiber orientation. It is necessary that the influence of these factors on the principal orientation angle and orientation intensity be clarified. In addition, the influence of the fiber diameter variation to the fiber orientation distribution should be investigated. Further experiments of the flow simulation are necessary to study the adaptability of the proposed PDF. If the fiber orientation can be evaluated more quantitatively, the tensile characteristics of FRCC can be estimated more precisely.

ACKNOWLEDGMENTS

The authors wish to express their gratitude and sincere appreciation to the Kuraray Co., Ltd. for providing the PVA fiber. The tension test was performed in the cooperation with Mr. Ryoichi Tsukizaki, a former student in the master's program of University of Tsukuba. This study was supported by the JSPS KAKENHI Grant Number 24656319.

REFERENCES

1. Bentur, A., and Mindess, S., "Fiber Reinforced Cementitious Composites", *Elsevier Applied Science*, London, UK, 1990.
2. Balaguru, P., and Shah, S. P., "Fiber Reinforced Cement Composites", McGraw Hill, New York, 1992.
3. Naaman, A. E., and Reinhardt, H. W., Co-Editors, "High Performance Fiber Reinforced Cement Composites: HPFRCC 2", *RILEM Proc.*, No.31, E. & FN Spon, London, 1996.
4. Li, V. C., "From Micromechanics to Structural Engineering – the Design of Cementitious Composites for Civil Engineering Applications", *JSCE Journal of Structural Mechanics and Earthquake Engineering*, Vol.10, No.2, pp.37-48, 1993.
5. Kanda, T., and Li, V. C., "Effect of Fiber Strength and Fiber-Matrix Interface on Crack Bridging in Cement Composites", *ASCE Journal of Engineering Mechanics*, Vol.125, No.3, pp.290-299, 1999.
6. Li, V. C., and Leung, C. K. Y., "Steady-State and Multiple Cracking of Short Random Fiber Composites", *ASCE Journal of Engineering Mechanics*, Vol.118, No.11, pp.2246-2264, 1992.
7. Rokugo, K., and Kanda, T., Co-Editors, "Strain Hardening Cement Composites: Structural Design and Performance", *State-of-the-Art Report of the RILEM Technical Committee 208-HFC, SC3*, Springer, 2013.

8. Laranjeira, F., Aguado, A., Molins, C., Grünewald S., Walraven, J., and Cavalaro, S., "Framework to predict the orientation of fibers in FRC: A novel philosophy", *Cement and Concrete Research*, 42, pp.752-768, 2012.
9. Kanakubo, T., "Tensile Characteristics Evaluation Method for Ductile Fiber-Reinforced Cementitious Composites", *Journal of Advanced Concrete Technology*, Vol.4, No.1, pp.3-17, 2006.
10. Li, V. C., and Wang, S., "On High Performance Fiber Reinforced Cementitious Composites", *JCI Proceedings of the Symposium on Ductile Fiber-Reinforced Cementitious Composites*, pp.13-23, 2003.
11. Naaman, A., "A Statistical Theory of Strength for Fiber Reinforced Concrete", Ph.D. dissertation, Massachusetts Institute of Technology, Cambridge, MA, pp.1-196, 1972.
12. Stroeven, P., "Stereological Principles of Spatial Modeling Applied to Steel Fiber-Reinforced Concrete in Tension", *ACI Materials Journal*, Vol.106, No.3, pp.213-222, 2009.
13. Dupont, D., and Vandewalle, L., "Distribution of steel fibres in rectangular sections", *Cement & Concrete Composites*, 27, pp.391-398, 2005.
14. Xia, J., and Mackie, K., "Axisymmetric Fiber Orientation Distribution of Short Straight Fiber in Fiber-Reinforced Concrete", *ACI Materials Journal*, Vol.111, No.2, pp.133-141, 2014.
15. Liu, J., Li, C., Liu, J., Cui, G., and Yang, Z., "Study on 3D Spatial Distribution of Steel Fibers in Fiber Reinforced Cementitious Composites through Micro-CT Technique", *Elsevier Construction and Building Materials*, Vol.48, pp.656-661, 2013.
16. Torigoe, S., Saito, T., Horikoshi, T., Hamada, T., and Ogawa, A., "Study on Evaluation Method for PVA Fiber Distribution in Engineered Cementitious Composite",

Proceedings of the JCI International Workshop on Ductile Fiber Reinforced Cementitious Composites, pp.95-101, 2002.

17. Kanda, T., Tomoe, S., Nagai, S., Maruta, M., Kanakubo, T., and Shimizu, K., "Full Scale Processing Investigation for ECC Pre-Cast Structural Element", *Journal of Asian Architecture and Building Engineering*, Vol.5, No.2, pp.333-340, 2006.
18. Japan Society of Civil Engineers, "Standard Specifications for Concrete Structures -2013, Test Methods and Specifications", *JSCE Standard*, pp.281-282, 2013 (in Japanese).
19. Enomae, T., Han, Y. H., and Isogai, A., "Fiber orientation distribution of paper surface calculated by image analysis", *Proceedings of International Papermaking and Environment Conference*, Tianjin, P.R. China (May 12-15), Book 2, pp.355-368, 2004.
20. Kanda, T., and Li, V. C., "Interface Property and Apparent Strength of High-Strength Hydrophilic Fiber in Cement Matrix", *ASCE Journal of Materials in Civil Engineering*, Vol.10, No.1, pp.5-13, 1998.
21. Redon, C., Li, V. C., Wu, C., Hoshiro, H., Saito, T., and Ogawa, A., "Measuring and Modifying Interface Properties of PVA Fibers in ECC Matrix", *ASCE Journal of Materials in Civil Engineering*, Vol.13, No.6, pp.399-406, 2001.
22. Kiyota, M., Mihashi, H., Kanda, T., and Kawamata, A., "Study on Bond Characteristics of Fibers in Cementitious Composites", *JCI Proceedings of the Japan Concrete Institute*, Vol.23, No.2, pp.187-192, 2001 (in Japanese).
23. Yang, E. H., Wang, S., Yang, Y., and Li, V. C., "Fiber-Bridging Constitutive Law of Engineered Cementitious Composites", *Journal of Advanced Concrete Technology*, Vol.6, No.1, pp.181-193, 2008.
24. Li, V. C., Wang, Y., and Backer, S., "A Micromechanical Model of Tension-Softening and Bridging Toughening of Short Random Fiber Reinforced Brittle Matrix Composites", *J. Mech. Phys. Solids*, Vol.39, No.5, pp.607-625, 1991.

TABLES AND FIGURES

List of Tables:

List of Figures:

Table 1 Mechanical properties of PVA fiber and target fiber

Type	Density, g/cm^3 (lb/ft^3)	Length, mm (in.)	Diameter, mm (in.)	Tensile strength, N/mm^2 (ksi)	Elastic modulus, kN/mm^2 (ksi)
PVA	1.30 (81.2)	12 (0.47)	0.10 (3.9×10^{-3})	1200 (174)	28 (4060)
Nylon	1.14 (71.2)	12 (0.47)	0.24 (9.3×10^{-3})	65 (9.4)	-

Table 2 Mix proportion of HPFRCC

Fiber volume fraction, %	Water by binder ratio	Sand by binder ratio	Unit weight, kg/m^3 (lb/yd^3)			
			Water	Cement	Fly ash	Sand
2.0	0.39	0.50	380 (641)	678 (1144)	291 (491)	484 (817)

Cement: High early strength Portland cement
Fly ash: Type II of Japanese Industrial Standard (JIS A 6202)
Sand: Size under 0.2 mm (7.9×10^{-3} in.)
Super plasticizer: Binder $\times$ 0.6 %

Table 3 Tension test results

Casting direction	ID	At cracking (First peak)		Max. after cracking (Second peak)	
		Tensile stress, N/mm^2 (ksi)	Crack width, mm (in.)	Tensile stress, N/mm^2 (ksi)	Crack width, mm (in.)
Horizontal	TH20-1*1	4.49 (0.651)	0.032 (0.0013)	3.70 (0.537)	0.460 (0.0181)
	TH20-2*1	4.41 (0.640)	0.034 (0.0013)	3.85 (0.558)	0.463 (0.0182)
	TH20-3*2	3.17 (0.460)	0.030 (0.0012)	2.97 (0.431)	0.446 (0.0176)
	Average	4.02 (0.583)	0.032 (0.0013)	3.51 (0.509)	0.456 (0.0180)
Vertical	TV20-1*1	3.53 (0.512)	0.023 (0.0009)	1.37 (0.199)	0.328 (0.0129)
	TV20-2*2	2.35 (0.341)	0.013 (0.0005)	1.55 (0.225)	0.177 (0.0070)
	TV20-3*2	3.53 (0.512)	0.030 (0.0012)	2.09 (0.303)	0.284 (0.0112)
	Average	3.14 (0.455)	0.022 (0.0009)	1.67 (0.242)	0.263 (0.0104)

*1: Batch #1, compressive strength 39.2 N/mm^2 (5.69 ksi)
*2: Batch #2, compressive strength 41.0 N/mm^2 (5.95 ksi)

Table 4 Previous PVA fiber pullout test results

Researcher	Water by cement ratio	Fiber diameter, mm (in.)	First peak load, N (lbf)	Second peak load, N (lbf)
Kanda et al. (1998) [20]	0.27	0.014 (0.55×10^{-3})	0.05 – 0.25 (0.011 – 0.056)	-
	0.42		0.12 – 0.20 (0.027 – 0.045)	-
	0.62		0.07 – 0.14 (0.016 – 0.031)	-
Redon et al. (2001) [21]	0.30	0.044 (1.7×10^{-3})	0.8 – 1.2 (0.18 – 0.27)	1.1 – 1.6 (0.25 – 0.36)
Kiyota et al. (2001) [22]	0.34	0.038 (1.5×10^{-3})	0.3 – 0.6 (0.07 – 0.13)	0.5 – 1.3 (0.11 – 0.29)
	0.42		0.4 – 0.6 (0.09 – 0.13)	0.4 – 1.3 (0.09 – 0.29)
	0.62		0.2 – 0.4 (0.04 – 0.09)	0.4 – 0.9 (0.09 – 0.20)
Yang et al. (2008) [23]	0.58	0.039 (1.5×10^{-3})	0.3 – 0.6 (0.07 – 0.13)	0.5 – 1.0 (0.11 – 0.22)

Table 5 Parameters for bridging law

Parameter			Input value	Remarks
First peak load, P_a, N (lbf)			1.5 (0.34)	*1
Crack width at P_a, δ_a, mm (in.)			0.2 (7.8×10^{-3})	0.1 mm (3.9×10^{-3} in.)*1 × 2
Maximum load, P_{max}, N (lbf)			3.0 (0.67)	*1
Crack width at P_{max}, δ_{max}, mm (in.)			0.45 (18×10^{-3})	0.3 mm (12×10^{-3} in.)*1 × 1.5
Fiber strength, σ_{fu}, N/mm² (ksi)			774 (112)	1200 N/mm² (174 ksi) × 0.645 *2
Snubbing coeffient, f			0.5	*2
Fiber strength reduction factor, f'			0.3	*2
x-y plane	Orientation intensity, k_{xy}	Horizontal casting	1.5	Value near to V_f 1.5 % and 2.0% visualizations
		Vertical casting	0.5	
	Principal orientation angle, $\theta_{r,xy}$		0	For calculation simplification *3
z-x plane	Orientation intensity, k_{zx}	Horizontal casting	6	Value near to V_f 1.5 % and 2.0% visualizations
		Vertical casting	0.5	
	Principal orientation angle, $\theta_{r,zx}$		0	For calculation simplification *3

PVA fiber: 0.10 mm (3.9×10^{-3} in.) diameter, 12 mm (0.47 in.) length.
*1: Assumed value based on Kiyota et al. (2001) [22] and Yang et al. (2008) [23]
*2: Assumed value for PVA fiber by Kanda et al. (1999) [5]
*3: Approximately average value of all V_f visualizations

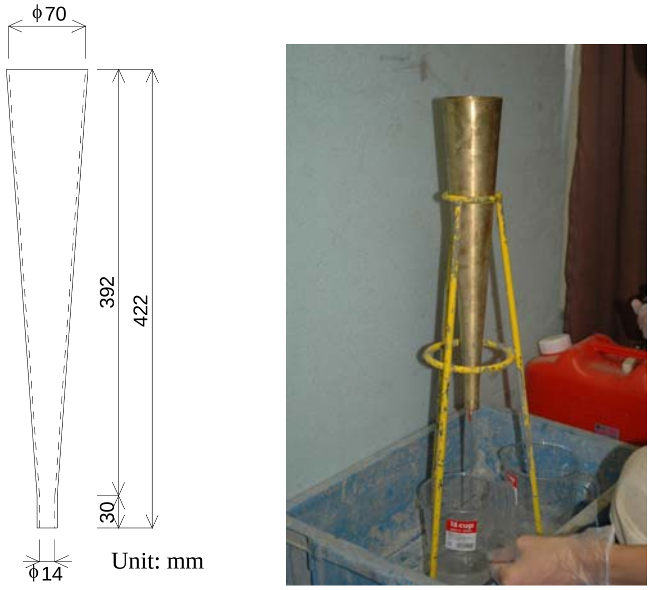

Fig. 1 Flowability test using the funnel (Note: 1 mm = 0.0394 in.)

(a) PVA fiber **(b) Target fiber**

Fig. 2 Mixing of fiber in water glass

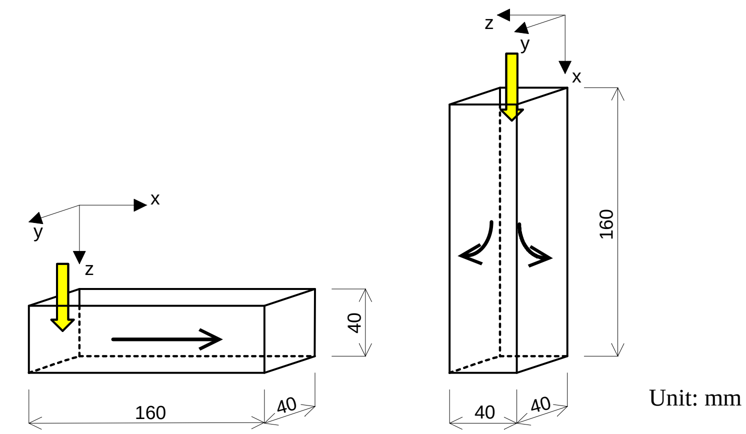

(a) Horizontal casting **(b) Vertical casting**

Fig. 3 Mold for visualization simulation (Note: 1 mm = 0.0394 in.)

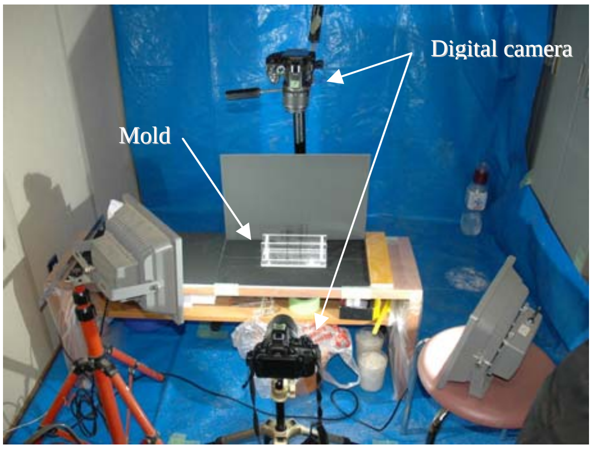

Fig. 4 Camera setup (horizontal casting)

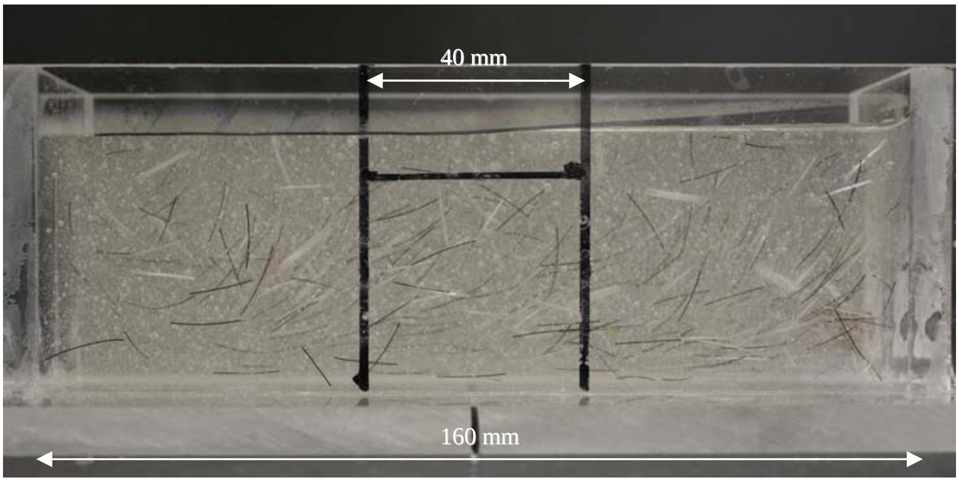

Fig. 5 Example of photograph (V_f = 0.1%, horizontal, z-x) (Note: 1 mm = 0.0394 in.)

(a) Cropping **(b) Binarization** **(c) Labelling**

Fig. 6 Image analysis procedures (Note: 1 mm = 0.0394 in.)

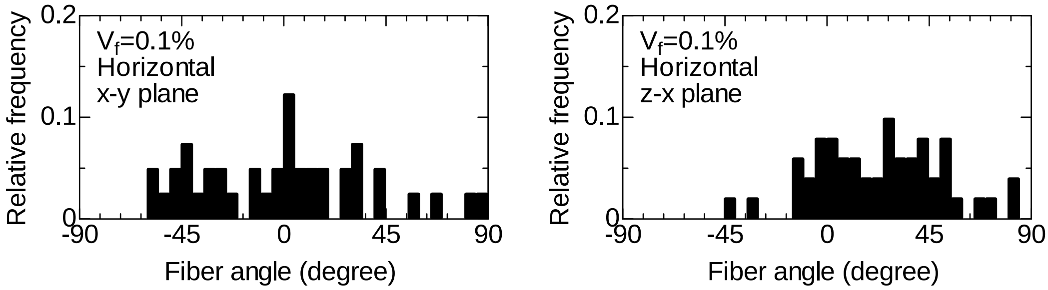

Fig. 7 Examples of fiber angle histograms

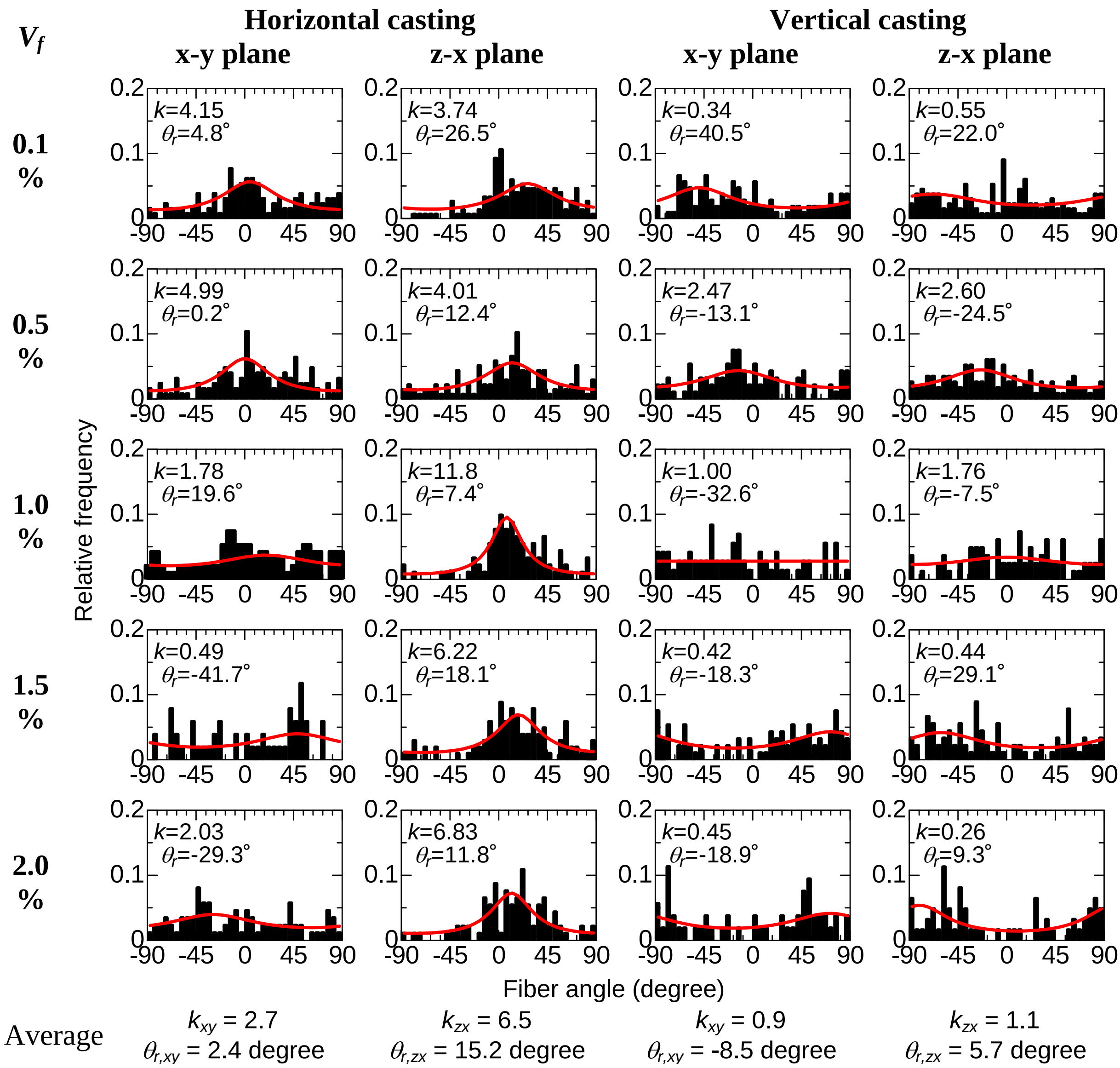

Fig. 8 All fiber angle histograms

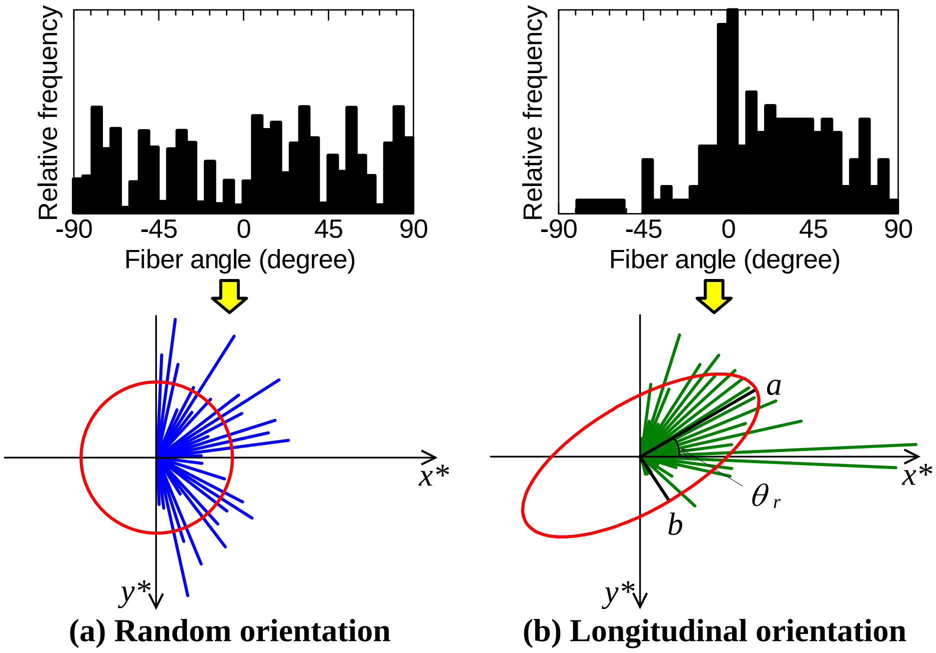

Fig. 9 Approximation method based on elliptic function

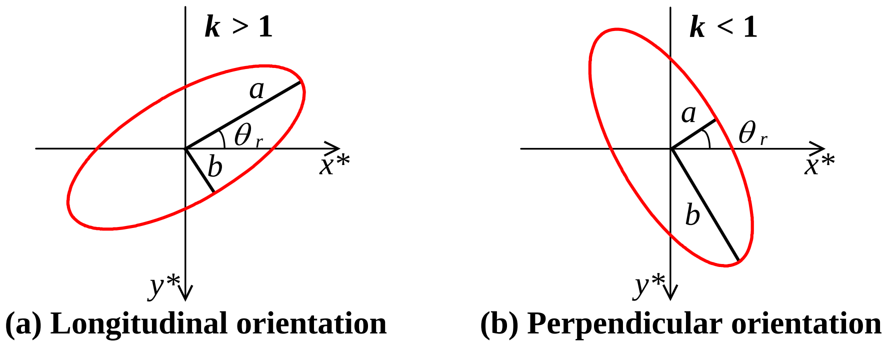

Fig. 10 Definition of principal orientation angle and orientation intensity

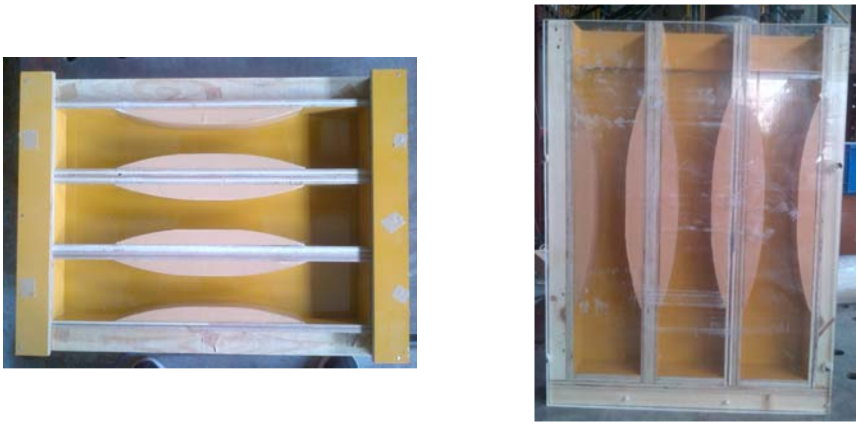

(a) Horizontal casting **(b) Vertical casting**

Fig. 11 Molds for tensile test specimen

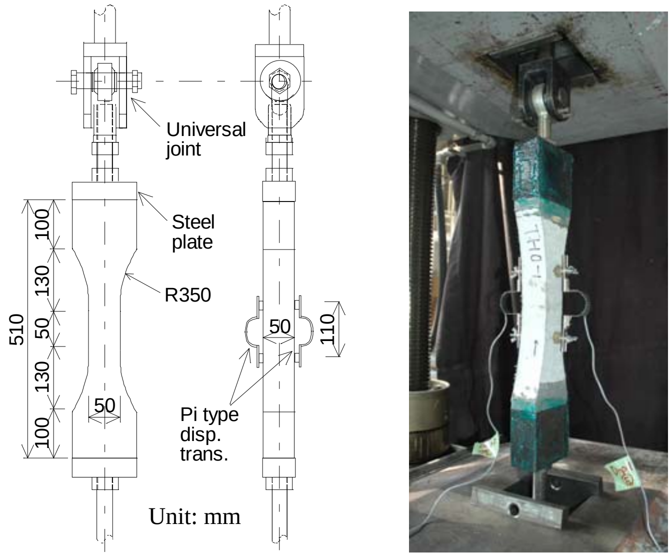

Fig. 12 Tensile test specimen (Note: 1 mm = 0.0394 in.)

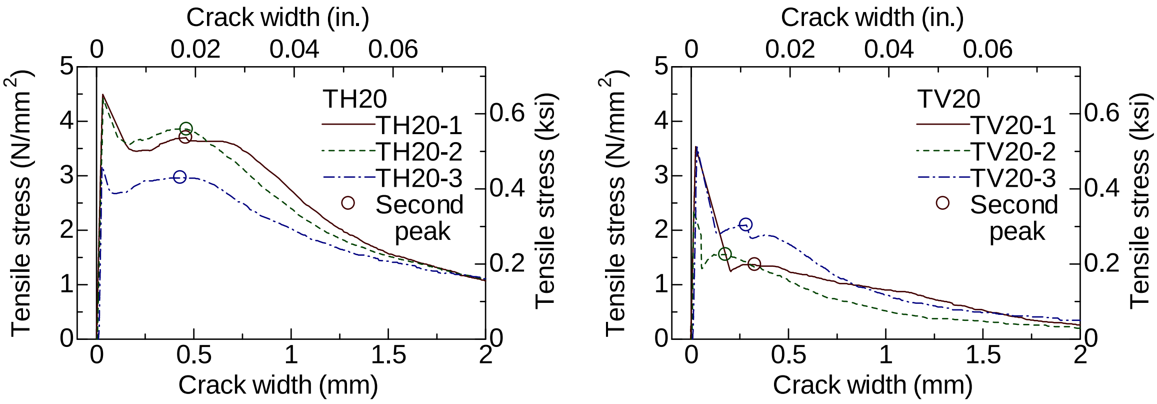

Fig. 13 Tensile stress – crack width curve

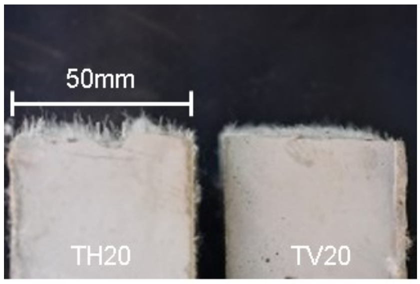

Fig. 14 Fracture surface after loading (Note: 1 mm = 0.0394 in.)

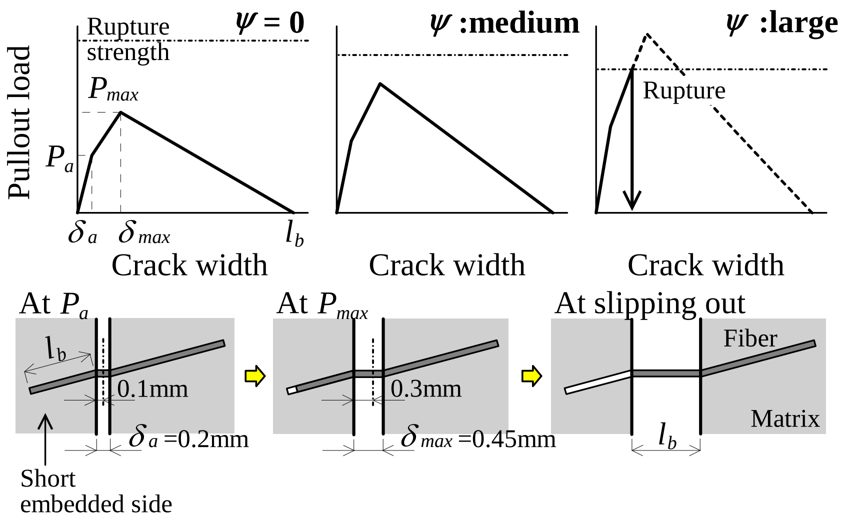

Fig. 15 Trilinear model for pullout load (Note: 1 mm = 0.0394 in.)

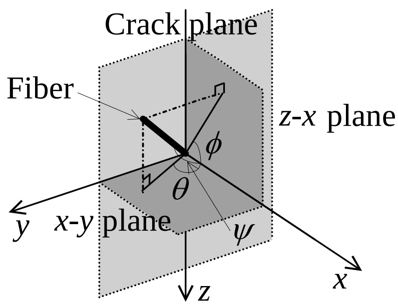

Fig. 16 Definitions of the coordinate system and fiber angle

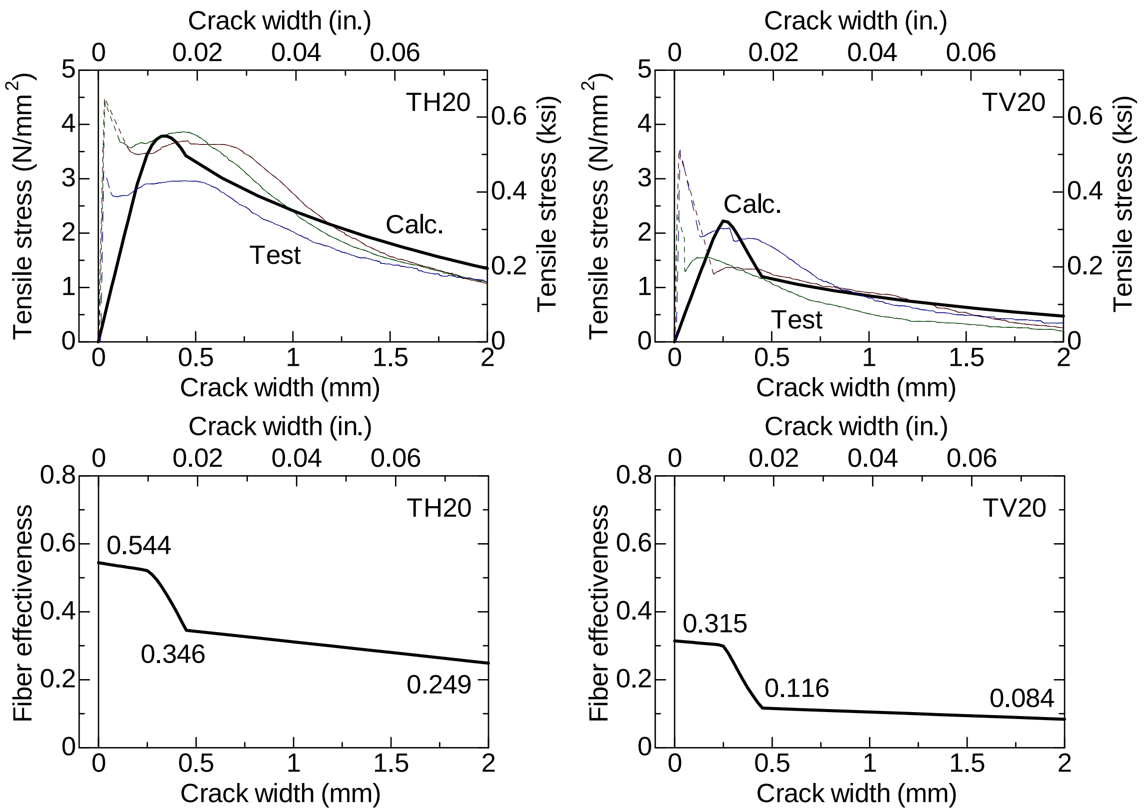

Fig. 17 Calculated bridging law and fiber effectiveness